Mapping ET at High Resolution in an Advective Semi-Arid Environment with Airborne Multispectral Imagery

J.L. Chávez[1], Ph.D., A.M.ASCE, P.H. Gowda[2], Ph.D. A.M.ASCE, T.A. Howell[2], Ph.D., F. ASCE, L.A. Garcia[1], Ph.D., M.ASCE, and K.S. Copeland[2]

[1]Colorado State University, Department of Civil and Environmental Engineering, 1372 Campus Delivery, Fort Collins, Colorado 80523-1372; Ph: (970) 491-6095; Fax: (970) 491-7727; Email: Jose.Chavez@ColoState.edu, and Luis.Garcia@ColoState.edu

[2]USDA-ARS, Conservation and Production Research Laboratory, P.O. Drawer 10, Bushland, Texas 79012-0010; Ph: (806) 356-5724; Fax (806) 356-5750; prasanna.gowda@ars.usda.gov, terry.howell@ars.usda.gov, and karen.copeland@ars.usda.gov

Abstract

Periodic and accurate estimates of spatially distributed evapotranspiration (ET) are essential for managing water in irrigated regions and in hydrologic modeling. In this study, METRIC (Mapping ET at high Resolutions with Internal Calibration), an energy balance algorithm originally developed for application with Landsat imagery at a regional scale, was applied to very high resolution aircraft imagery (0.5-2 m pixels) in the Texas High Plains. ET predictions were evaluated using data from four large precision weighing lysimeters located in the USDA-ARS Conservation and Production Research Laboratory, Bushland, Texas. Statistical results indicated that METRIC worked better for crops with leaf area index greater than 2.5 m^2 m^{-2}. Potential limitations may have been the areal extent of the imagery, the surface roughness for the momentum transfer sub-model, and the lack of a cold pixel with characteristics similar to the reference crop, i.e. alfalfa.

Introduction

Remote sensing (RS) derived ET maps can potentially be used in the monitoring of spatially distributed crop water use, to schedule irrigations, and as input for hydrologic models. Also, spatially distributed seasonal ET may be used to assess the water use efficiency of irrigation projects. Spatially distributed ET has been estimated using land surface energy balance (EB) models using RS multispectral imagery and ground-based micro-meteorological data. Gowda et al. (2008) and Gowda et al. (2007) present a description and discussion on most of the RS-based EB models available in the literature. Most of these EB models are single source models, e.g. SEBI (Menenti and Choudhury, 1993), SEBAL (Bastiaanssen et al., 1998), SEBS (Su, 2002), METRIC (Allen et al., 2007a), ReSET (Elhaddad and Garcia, 2008).

Of all these algorithms, METRIC may have an advantage under advective conditions. METRIC's ET estimation errors were reported to be approximately 10 to 20% for

daily estimates and as low as 1 to 4% for seasonal ET estimates (Trezza, 2002; Allen et al., 2007b; Chávez et al., 2009) for a semi-arid environment. Therefore, the attributes presented by METRIC make it very attractive for mapping ET in the Southern High Plains (SHP) where advective conditions are regularly encountered. The SHP is a semi-arid region with heterogeneous landscapes in which irrigated fields are surrounded by dryland crops, fallow land, and/or rangeland. Therefore, the advection of hot air from dry surfaces is a significant source of energy that has a major impact on ET from irrigated areas. For example, Tolk et al. (2006) reported an average ET rate of 11.3 mm d^{-1}, measured with a large weighing lysimeter, for irrigated alfalfa in Bushland, Texas, with ET for some days exceeding 15 mm d^{-1} due to regional advection. However, METRIC has not been applied using very high resolution (0.5-2 m pixel) airborne imagery. METRIC was adapted from SEBAL (Surface Energy Balance Algorithm for Land) and was used with satellite imagery, Landsat 5/7, with pixel spatial resolutions in the order of 30-120 m.

In this study, the objectives were: a) to apply METRIC to the advective semi-arid SHP environment, using very high spatial resolution (0.5-2 m pixel) airborne RS imagery and ground-based meteorological data, and b) to evaluate METRIC estimated daily ET values using large precision weighing lysimeters.

Material and Methods

Study Area

This study was conducted at the USDA-ARS Conservation and Production Research Laboratory (CPRL) located in Bushland, Texas. The geographic coordinates of the CPRL are [35º 11' N, 102º 06' W], and its elevation is 1,170 m above mean sea level. Soils in and around Bushland are classified as slowly permeable Pullman clay loam. The major crops in the region are corn, sorghum, winter wheat, and cotton.

Remote Sensing System and Data

The RS system used in this study was the Utah State University (USU) airborne digital multispectral system. The USU RS system acquired high resolution imagery in the visible, near-infrared, and thermal-infrared portions of the electromagnetic spectrum. The USU multispectral system was comprised of three Kodak[1] Megaplus digital frame cameras (Eastman Kodak Company, Rochester, New York) with interference filters centered in the green (Gn) (0.545-0.560 μm), red (R) (0.665-0.680 μm), and near-infrared (NIR) (0.795-0.809 μm) portions of the electromagnetic spectrum. The fourth camera was an Inframetrics 760 (Inframetrics, N. Billerica, MA) thermal-infrared scanner radiometer (8-12 μm) that provides thermal-infrared (TIR) imagery, used to obtain surface radiometric temperature images. The USU airborne digital multispectral system flew at an altitude of about 1,000 m (above

[1] The mention of trade names of commercial products in this article is solely for the purpose of providing specific information and does not imply recommendation or endorsement by the U.S. Department of Agriculture or Colorado State University.

ground level), which resulted in a 0.5 m pixel resolution for the visible and NIR bands and 1.8 m for the TIR band.

Six airborne RS images acquired over the CPRL during the 2007 cropping season, on June 25 (DOY 176), July 3 (DOY 184), July 10 (DOY 191), July 11 (DOY 192), July 26 (DOY 207), and August 11 (233), were used in this study (e.g., Fig. 1). All images were acquired close to 11:30 AM CST, except on DOY 184 in which the image was acquired close to 9:00 AM CST. These images were calibrated and transformed into surface reflectance and temperature images for estimating reflected outgoing shortwave and longwave radiation, respectively, with both components required in the estimation of spatially distributed net radiation.

Radiometric and Atmospheric Calibration of Aircraft Data

The shortwave images were corrected for lens vignetting effects and geometric distortions using procedures similar to those described by Neale and Crowther (1994) and Sundararaman and Neale (1997). The individual R, Gn, and NIR images were registered into three band images and rectified to a digital orthophotoquad base map.

The digital numbers of the rectified multispectral image were converted to radiance using the system calibration method described in Neale and Crowther (1994). These radiances were divided by the incoming solar irradiance to obtain surface spectral reflectance. Solar irradiance in each spectral band was obtained from radiance measurements made concurrently to the flights with an Exotech radiometer placed over a barium sulfate standard reflectance panel with known bidirectional properties (Jackson et al., 1992).

The TIR imagery was rectified to the high-resolution three-band images described above. The digital numbers were transformed into apparent (at sensor or brightness) temperature values using the Inframetrics 760 thermal scanner system calibration bar at the bottom of each image. The surface brightness temperature images were corrected for atmospheric effects considering surface thermal emissivity and using the atmospheric radiative transfer model MODTRAN4 v3 (Berk et al., 2003). These corrections resulted in at-surface radiometric temperatures (T_s).

METRIC Model-based Remote Sensing ET

In METRIC, ET is computed as a residual from the surface EB equation as an instantaneous ET or latent heat flux (LE; Brown and Rosenberg, 1973; and Stone and Horton, 1974), Equation (1).

$$R_n = G + H + LE \tag{1}$$

where R_n is net radiation (W m^{-2}) calculated using T_s, near surface vapor pressure from a near-by weather station (WS), and R_s as explained below. G is soil heat flux (W m^{-2}), and H is sensible heat flux (W m^{-2}). R_n was computed using the following equation:

$$R_n = R_s \downarrow - \alpha R_s \downarrow + R_L \downarrow - R_L \uparrow - (1 - \varepsilon_o) R_L \downarrow \tag{2}$$

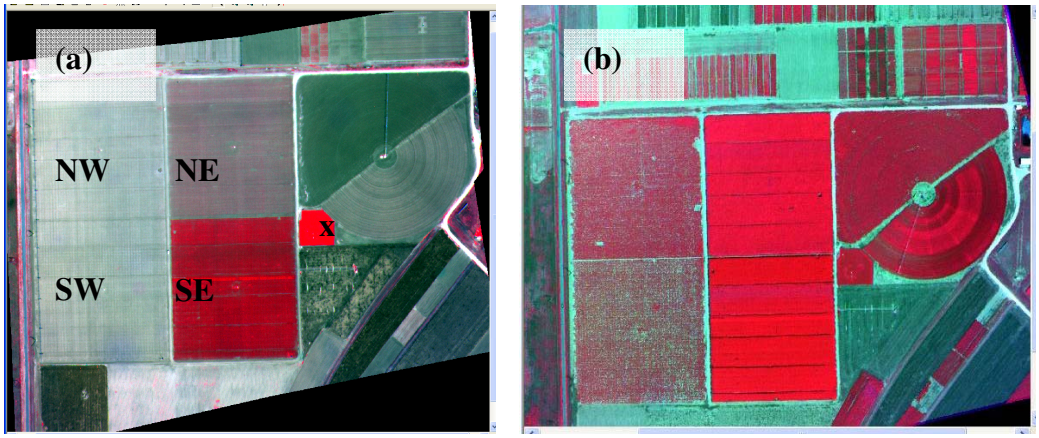

Figure 1. False color (NIR, R, Gn) composite reflectance images for (a) DOY 176 and (b) DOY 223. Lysimeter fields NW, NE, SE, and SW plus the weather station location (x) are shown in image (a) for DOY 176.

where $R_s\downarrow$ is incoming shortwave radiation (W m^{-2}). In this study, $R_s\downarrow$ was not estimated as indicated in Allen et al. (2002, 2007a) but rather measured with a pyranometer (model CMP 6, Kipp and Zonen, Bohemia, NY) installed at the USDA-ARS-CPRL weather station (TXHPET, 2006). Surface albedo, α, was estimated following Brest and Goward (1987). $R_L\downarrow$ is incoming long wave radiation (W m^{-2}) or downward thermal radiation flux originated from the atmosphere, which was estimated using the Stefan-Boltzmann equation and near surface air temperature as well as vapor pressure and sky emissivity. Sky/air/atmospheric thermal emissivity was estimated according to Brutsaert (1975). $R_L\uparrow$ is outgoing long wave radiation (W m^{-2}), a function of T_s and surface thermal emissivity (ε_o, dimensionless). The ε_o term was estimated according to Brunsell and Gillies (2002).

Soil heat flux (G) is a function of R_n, a vegetation index, T_s, and α (Bastiaanssen, 2000):

$$G = ((T_s - 273.15)\,(0.0038+0.0074\,\alpha)\,(1-0.98\,NDVI^4))\,R_n \qquad (3)$$

where NDVI is the Normalized Difference Vegetation Index [(R-NIR)/(R+NIR)], R is reflectance in the red band and NIR is reflectance in the near infrared band.

Sensible heat flux (H) is defined by the bulk aerodynamic resistance equation.

$$H = \rho_a Cp_a \frac{dT}{r_{ah}} \qquad (4)$$

where ρ_a is air density (kg m^{-3}), Cp_a is specific heat of dry air (1004 J kg^{-1} K^{-1}), dT (K) is a function of T_s, ($dT = a + b\,T_s$; Bastiaanssen, 1995) representing a near surface temperature difference between z_1 and z_2, and r_{ah} is aerodynamic resistance (s m^{-1}),

calculated between two near surface heights, z_1 and z_2 (0.1 and 2.0 m) using a wind speed extrapolated from a blending height above the ground surface (200 m) and an iterative stability correction scheme for atmospheric heat transfer based on the Monin-Obhukov stability length scale ($L_{_MO}$, similarity theory; Foken, 2006).

The determination of *a* and *b* (in dT) involves locating a hot (dry) pixel in a fallow agricultural field with large T_s and a cold (wet) pixel with a small T_s (irrigated field) in the RS image. Then, the EB of Equation (1) can be solved for H_{cold} and H_{hot} as $\boldsymbol{H_{cold} = (R_n - G)_{cold} - LE_{cold}}$, and as $\boldsymbol{H_{hot} = (R_n - G)_{hot} - LE_{hot}}$, respectively. H_{hot} and H_{cold} are the sensible heat fluxes for the hot and cold pixels, respectively. The hot pixel is defined as having $LE_{hot} = 0$, which means that all available energy is partitioned to H. In METRIC, the cold pixel is assumed to have an LE value equal to 1.05 times that expected for a tall reference crop (i.e., alfalfa), thus LE_{cold} is set equal to 1.05 ET_r λ_{LE}, where ET_r is the hourly tall reference ET calculated using the standardized ASCE Penman-Monteith equation (ASCE-EWRI, 2005).

The hot pixel was chosen in a fallow agricultural field displaying high temperatures, high albedo and low biomass (low LAI). Thus, with the calculation of H_{hot} and $H_{cold,}$ Equation (4) was inverted to compute dT_{hot} and dT_{cold}. The *a* and *b* coefficients were then determined by fitting a line through the two pairs of values for dT and T_s from the hot and cold pixels. These *a* and *b* values were initial estimates that were used in an iterative stability correction scheme programmed in a Microsoft Excel™ spreadsheet, which after some iterations shows numerical convergence. The *a* and *b* coefficients for each iteration were then exported to a model in ERDAS IMAGINE® (ERDAS, Inc., Norcross, GA) to obtain the final stability corrected H image.

Instantaneous LE image values were obtained using Equation (1) and were converted to hourly ET (ET_i) in mm h^{-1} by dividing LE by λ_{LE} and ρ_w, as follows:

$$ET_i = 3600\ LE\ /\ \{[2.501 - 0.00236\ (T_s - 273.15)]\ (10^6)\ (1.0)\} \tag{5}$$

Reference ET fraction (ET_rF) is the ratio of ET_i to the alfalfa reference ET (ET_r) that is computed from WS data at overpass time (hourly average). Finally, the computation of daily or 24-h ET (ET_d), for each pixel, was performed as:

$$ET_d = ET_rF \times ET_r24 \tag{6}$$

where ET_r24 is the cumulative 24-h ET_r for the day (mm d^{-1}).

Verification of estimated daily ET values

Estimated daily ET values were verified by comparison with measured ET with four large monolithic weighing lysimeters located at the CPRL. The lysimeters (3×3×2.4 m) were situated in the middle of 4.7-ha fields. In 2007, the lysimeter fields, northeast (NE, Fig. 1) was planted to forage sorghum (planted on May 30), the southeast (SE, Fig. 1) was planted to corn (planted on May 17) both for silage production, the

northwest (NW, Fig. 1) was planted to grain sorghum in rows (planted on June 6), while the southwest (SW, Fig. 1) lysimeter field was planted to grain sorghum (planted on June 6) in clumps as part of another ongoing research project. Furthermore, the NE and SE lysimeter fields were irrigated while the NW and SW lysimeter fields were managed under dryland conditions. Each lysimeter field was equipped with one net radiometer [Q*7.1, Radiation and Energy Balance Systems (REBS), Bellevue, WA] and one infra-red thermometer, (Exergen, Watertown, MA) for measuring R_n and surface temperature, respectively.

Errors between estimated and observed ET values were reported as mean bias errors (MBE) and root mean square errors (RMSE). Besides ET, predicted instantaneous net radiation (R_n) was verified with measured data and differences were reported as MBE and RMSE.

Results and Discussion

Net Radiation Estimation

Remote sensing based R_n compared well with observed R_n as shown in Fig. 2. Net radiation was estimated with a small average under prediction error/bias of -17 W m^{-2} (-2.8%) and a RMSE of 48 W m^{-2} (7.9% of the observed mean); which shows a small error spread. Larger under estimation occurred when observed R_n values were larger than 700 W m^{-2} (Fig. 2). The error perhaps was due, in part, by error in the estimation of surface albedo for large biomass (LAI), closed canopy conditions. Nevertheless, it is an overall small error.

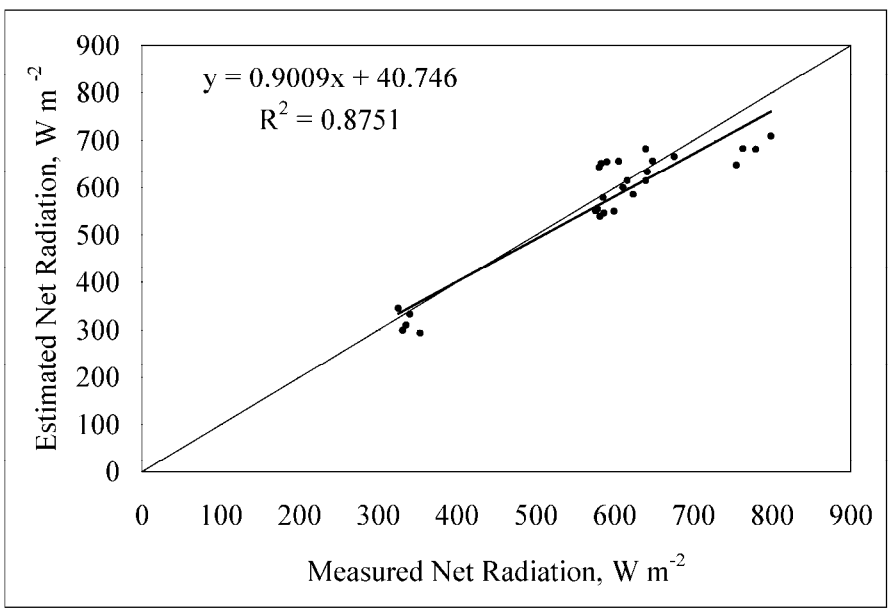

Figure 2. Estimated vs. observed instantaneous net radiation comparison.

Daily ET Estimation

METRIC underestimated daily ET with a MBE of -0.2 mm d^{-1} (-6.9%) and a RMSE of 1.9 mm d^{-1} (-40.1%). Although, Fig. (3) shows that the underestimation occurred on ET values ranging from 2 to 6 mm d^{-1} while an overestimation occurred for measured ET values larger than 6 mm d^{-1}. In part, errors in estimating ET may have been due to errors in locating true hot and cold pixels, i.e. true hot and cold pixels (extreme temperature pixels) may fall outside of the area covered by the aircraft overpasses. The areal extent of the airborne imagery used in this study was approximately 800 m (E-W direction) by 650 m (N-S direction) while a Landsat 5 Thematic Mapper (TM) scene covers an area of 170 km (N-S) by 183 km (E-W).

Errors associated with the selection of the cold pixel in the irrigated grass field of the ARS weather station location could have been another potential source of error. The grass height was kept at about 0.12 m; however, METRIC indicates selecting the cold pixel on a field with crop characteristics (height and LAI) similar to the alfalfa reference crop. This selection was not possible on DOY 176 and 184 because, all other fields covered in the airborne imagery were drier/warmer than the reference WS grass field.

The absolute differences (in %) between estimated and measured ET were plotted versus LAI in Fig. (4). As shown in Fig. (4), most large errors in ET (larger than 40%) occurred at LAI values smaller than 2.5 m^2 m^{-2}. Coincidently, most of these low LAI values showed the largest surface temperature. See Fig. (5). Although, there were some data points showing much cooler temperatures (circle) at low LAI values in Fig. (5). This latter fact may be attributed to an irrigation event (approx. 18 mm, to keep the sorghum alive) on DOY 184 on the NW and SW dryland lysimeter fields, and to a rainfall event on DOY 192 (approx. 15.5 mm) that lowered the temperature of these fields.

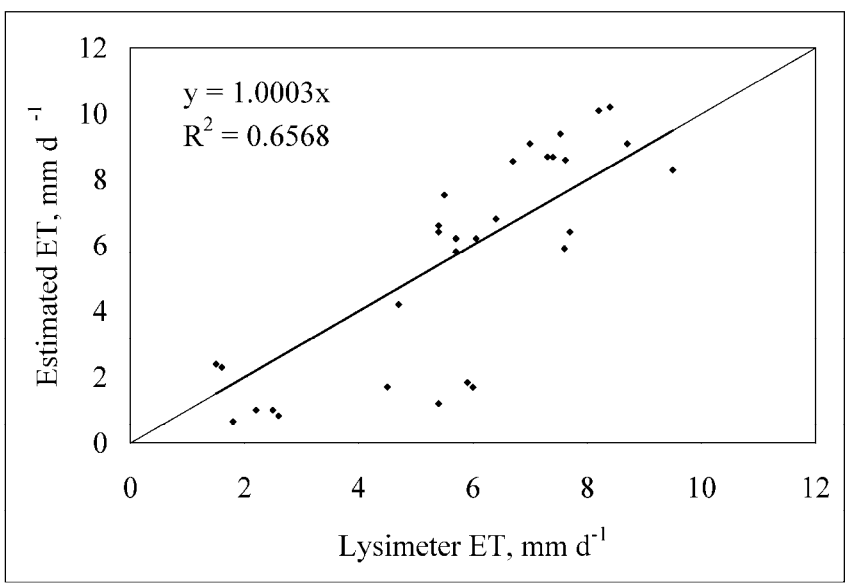

Figure 3. METRIC estimated ET vs. Lysimeter measured ET.

Therefore, the larger ET underestimation (circle in Fig. 4) occurred for LAI values smaller than 2.5 m^2 m^{-2} on DOY 184 and 192 when the sparse sorghum fields were wet. Under these conditions, the estimation of the roughness length for momentum transfer (Z_{om}), friction velocity (u_*), and aerodynamic resistance (r_{ah}) may have been compromised, resulting in errors in the estimation of H_{hot} and hence in ET.

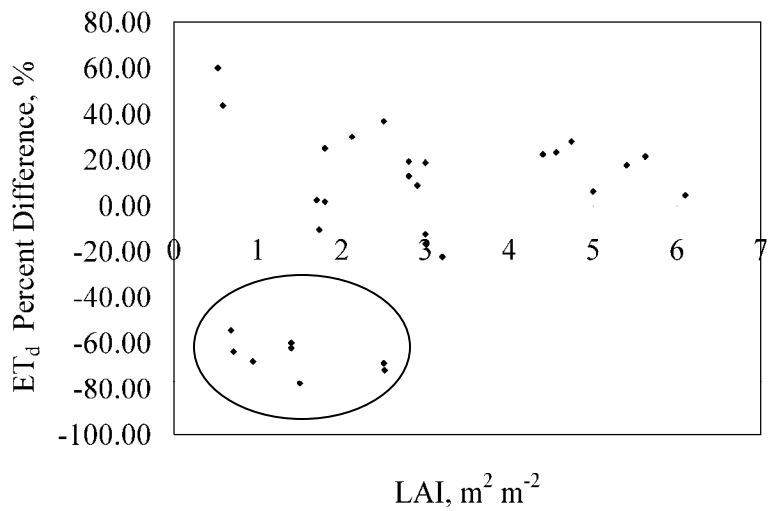

Figure 4. Percent ET error vs. LAI.

METRIC estimated ET with a MBE of 0.6 mm d^{-1} (10.8%) and a RMSE of 1.2 mm d^{-1} (16.5%) when estimated ET values from those fields/crops with LAI smaller than 2.5 m^2 m^{-2} were excluded from the analysis.

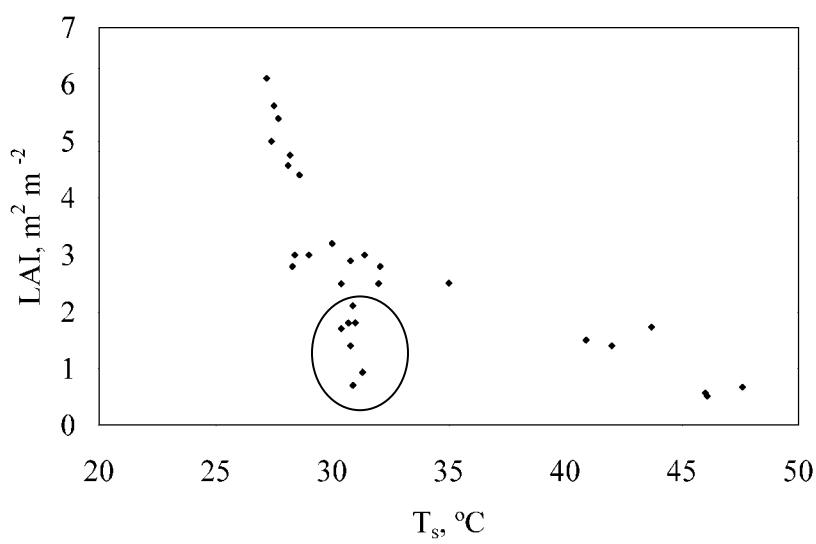

Figure 5. LAI vs. surface temperature (T_s).

Conclusions

METRIC was applied on six airborne RS images acquired over the CPRL during the 2007 cropping season over the semi-arid region of the Southern High Plains. There were large ET underestimation errors for crops with LAI values smaller than 2.5 m^2 m^{-2} under wet surface conditions. Removing ET values under those conditions reduced the error to 10.8±16.5% (an overestimation). It is hypothesized that the roughness length for momentum transfer (Z_{om}), friction velocity (u_*), and aerodynamic resistance (r_{ah}) may have not been well estimated under the conditions described above, resulting in errors in the estimation of H_{hot} and hence in ET. In addition, the areal extent covered by the airborne system may have prevented selecting true extreme cold and hot pixels. Moreover, selecting a cold pixel on a field with crop characteristics different from the alfalfa reference crop may result in a bias scaling of surface temperature in the dT function. Nonetheless, this result is encouraging. It is believed that by improving the Z_{om} sub-model and by enlarging the areal coverage of the airborne RS system, using multiple stitched images (mosaic), it may be possible to further improve the accuracy of ET estimates.

Acknowledgements

This study was possible thanks to funding provided through the Ogallala Aquifer Program. Our sincere appreciation goes to the following individuals who provided assistance: Donald A. Dusek, Kim Bush, and Dr. Christopher M.U. Neale.

References

Allen, R.G., M. Tasumi, and R. Trezza. 2007a. Satellite-based energy balance for mapping evapotranspiration with internalized calibration (METRIC)-model. *ASCE J. of Irrig. and Drain. Eng.* 133(4): 380-394.

Allen, R.G., M. Tasumi, A. Morse, R. Trezza, J.L. Wright, W. Bastiaanssen, W. Kramber, I. Lorite-Torres and C.W. Robison. 2007b. Satellite-based energy balance for mapping evapotranspiration with internalized calibration (METRIC)-Applications *ASCE J. of Irrig. and Drain. Eng.* 133(4): 395 - 406.

Allen, R.G., M. Tasumi, and R. Trezza. 2002. *METRIC™: mapping evapotranspiration at high resolution – application manual for Landsat satellite imagery*. University of Idaho, Moscow, ID.

ASCE-EWRI. 2005. The ASCE standardized reference evapotranspiration equation. Report by the American Society of Civil Engineers (ASCE) Task Committee on Standardization of Reference Evapotranspiration. Allen, R.G., I.A. Walter, R.L. Elliot, T.A. Howell, D. Itenfisu, M.E. Jensen, and R.L. Snyder (eds.), ASCE, 0-7844-0805-X, 204 pp., Reston, VA.

Bastiaanssen, W.G.M. 1995. Regionalization of surface flux densities and moisture indicators in composite terrain: A remote sensing approach under clear skies in Mediterranean climates. Ph.D. Dissertation, CIP Data Koninklijke Bibliotheek, Den Haag, The Netherlands, 273p.

Bastiaanssen, W.G.M., M. Menenti, R.A. Feddes, and A.A. Holtslang. 1998. A remote sensing surface energy balance algorithm for land (SEBAL): 1. Formulation. *J. of Hydrol.* 212-213:198-212.

Bastiaanssen, W.G.M. 2000. SEBAL-based sensible and latent heat fluxes in the irrigated Gediz Basin, Turkey. *J. of Hydrol.* 229:87-100.

Berk, A., G.P. Anderson, P.K. Acharya, M.L. Hoke, J.H. Chetwynd, L.S. Bernstein, E.P. Shettle, M.W. Matthew, and S.M. Adler-Golden. 2003. MODTRAN4 version 3 revision 1 user's manual. Air Force Research Laboratory, Space Vehicle Directorate, Air Force Materiel Command, Hanscom AFB, MA 01731-300, Hanscom.

Brest, C.L., and S.N. Goward. 1987. Driving surface albedo measurements from narrow band satellite data. *International Journal of Remote Sensing*, 8:351-367

Brown, K.W., and N.J. Rosenberg. 1973. A resistance model to predict evapotranspiration and its application to a sugar beet field. *Agron. J.* 65(3): 341-347.

Brunsell, N.A., and R. Gillies. 2002. Incorporating surface emissivity into a thermal atmospheric correction. *Photogramm. Eng. Remote Sens. J.* 68: 1263-1269.

Brutsaert, W., 1975. On a derivable formula for long-wave radiation from clear skies. Water Resour. Res. 11, 742-744.

Chávez, J.L., P.H. Gowda, T.A. Howell, and K.S. Copeland. 2009. Radiometric surface temperature calibration effects on satellite based evapotranspiration estimation. *Int'l J. of Remote Sens.* Accepted 21 June 2008. In Press.

Elhaddad, A., L.A. Garcia. 2008. Surface energy balance-based model to estimate evapotranspiration taking into account spatial variability in weather. *Journal of Irrigation and Drainage Engineering, ASCE*, 134(6): 681-689.

Foken, T. 2006. 50 Years of the Monin-Obukhov similarity theory. *Boundary-Layer Meteorol.* 119(3): 431-447.

Gowda, P.H., J.L. Chavez, P.D. Colaizzi, S.R. Evett, T.A. Howell, and J.A. Tolk. 2008. ET mapping for agricultural water management: Present status and challenges. *Irrig. Sci.* 26(3):223-237, DOI 10.1007/s00271-007-0088-6.

Gowda, P.H., J.L. Chávez, P.D. Colaizzi, S.R. Evett, T.A. Howell, and J.A. Tolk. 2007. Remote sensing based energy balance algorithms for mapping ET: Current status and future challenges. *Trans. ASABE* 50(5): 1639-1644.

Jackson, R.D., T.R. Clarke, and M.S. Moran. 1992. Bidirectional calibration results of 11 Spectralon and 16 BaSO4 reference reflectance panels. *Remote Sens. of Env.* 40: 231-239.

Menenti, M., and B.J. Choudhury. 1993. Parameterization of land surface evapotranspiration using a location dependent potential evapotranspiration and surface temperature range. In *Proc. Exchange Processes at the Land Surface for a Range of Space and Time Scales*. 561-568, Bolle HJ et al. (eds), IAHS Publ. 212.

Neale, C.M.U., and B. Crowther. 1994. An airborne multispectral video/radiometer remote sensing system: development and calibration. *Remote Sens. of Env.* 49(3): 187-194.

Stone, L.R., and M.L. Horton. 1974. Estimating evapotranspiration using canopy temperatures: Field evaluation. *Agron. J.* 66: 450-454.

Su, Z. 2002. The surface energy balance system (SEBS) for estimation of turbulent heat fluxes. *Hydrol. and Earth Syst. Sci.* 6:85-99.

Sundararaman, S., and C.M.U. Neale. 1997. Geometric calibration of the USU videography system. In *Proc. 16th Biennial Workshop in Videography and Color Photography for Resource Assessment*. American Society of Photogrammetry and Remote Sensing, Bethesda, MD.

Tolk, J.A., S.R. Evett, and T.A. Howell. 2006. Advection influences on evapotranspiration of alfalfa in a semiarid climate. *Agronomy Journal,* 98: 1646 - 1654.

Trezza, R. 2002. Evapotranspiration using a satellite-based surface energy balance with standardized ground control. PhD dissertation, Logan, Utah: Utah State University, Biological and Irrigation Engineering Department.

TXHPET. 2006. Texas High Plains Evapotranspiration Network. Available online at: http://txhighplainset.tamu.edu/index.jsp (accessed 4 September 2006).